

Hyperspectral imaging fluorescence excitation scanning for colon cancer detection

Silas J. Leavesley
Mikayla Walters
Carmen Lopez
Thomas Baker
Peter F. Favreau
Thomas C. Rich
Paul F. Rider
Carole W. Boudreaux

Hyperspectral imaging fluorescence excitation scanning for colon cancer detection

Silas J. Leavesley,^{a,b,c,*} Mikayla Walters,^a Carmen Lopez,^d Thomas Baker,^b Peter F. Favreau,^{a,c} Thomas C. Rich,^{b,c} Paul F. Rider,^e and Carole W. Boudreaux^f

^aUniversity of South Alabama, Department of Chemical and Biomolecular Engineering, 150 Jaguar Drive, SH 4129, Mobile, Alabama 36688, United States

^bUniversity of South Alabama, Department of Pharmacology, 5851 USA North Drive, MSB 3372, Mobile, Alabama 36688, United States

^cUniversity of South Alabama, Center for Lung Biology, 5851 USA North Drive, MSB 3340, Mobile, Alabama 36688, United States

^dUniversity of South Alabama, Medical Sciences Program, 5851 USA North Drive, MSB 3340, Mobile, Alabama 36688, United States

^eUniversity of South Alabama, Department of Surgery, 2451 Fillingim Street, Mastin Building, Suite 701, Mobile, Alabama 36617, United States

^fUniversity of South Alabama, Department of Pathology, 2451 Fillingim Street, Mobile, Alabama 36617, United States

Abstract. Optical spectroscopy and hyperspectral imaging have shown the potential to discriminate between cancerous and noncancerous tissue with high sensitivity and specificity. However, to date, these techniques have not been effectively translated to real-time endoscope platforms. Hyperspectral imaging of the fluorescence excitation spectrum represents new technology that may be well suited for endoscopic implementation. However, the feasibility of detecting differences between normal and cancerous mucosa using fluorescence excitation-scanning hyperspectral imaging has not been evaluated. The goal of this study was to evaluate the initial feasibility of using fluorescence excitation-scanning hyperspectral imaging for measuring changes in fluorescence excitation spectrum concurrent with colonic adenocarcinoma using a small pre-pilot-scale sample size. *Ex vivo* analysis was performed using resected pairs of colorectal adenocarcinoma and normal mucosa. Adenocarcinoma was confirmed by histologic evaluation of hematoxylin and eosin (H&E) permanent sections. Specimens were imaged using a custom hyperspectral imaging fluorescence excitation-scanning microscope system. Results demonstrated consistent spectral differences between normal and cancerous tissues over the fluorescence excitation range of 390 to 450 nm that could be the basis for wavelength-dependent detection of colorectal cancers. Hence, excitation-scanning hyperspectral imaging may offer an alternative approach for discriminating adenocarcinoma from surrounding normal colonic mucosa, but further studies will be required to evaluate the accuracy of this approach using a larger patient cohort. © 2016 Society of Photo-Optical Instrumentation Engineers (SPIE) [DOI: 10.1117/1.JBO.21.10.104003]

Keywords: endoscopy; spectral; colorectal; spectroscopy; optical biopsy; hyperspectral imaging fluorescence excitation.

Paper 160335SSPRR received May 25, 2016; accepted for publication Oct. 4, 2016; published online Oct. 28, 2016.

1 Introduction

Colorectal cancer is the second leading cause of cancer death in the United States.¹ Early detection may play a key role in reducing cancer mortality²—the end goal of most colorectal screening exams is to identify lesions prior to malignancy or tissue invasion.^{3,4} Endoscopic procedures are the standard method for colorectal screening. There are currently several complementary endoscopic technologies for colorectal exams: white light endoscopy (WLE), narrow-band imaging, autofluorescence imaging, and chromoendoscopy.^{5–7} Interestingly, although the specificity and sensitivity of these endoscopic technologies have been estimated in a range of studies,^{3,5,6,8–11} no single technology has emerged as clearly superior. As such, WLE remains the gold standard and is often the “de facto” imaging modality for colorectal screening. However, recent studies have identified a need for improved screening effectiveness, showing that current methods are limited in their ability to detect flat⁶ or small (<5 mm diameter) lesions.^{3,12,13} Two studies suggest that flat adenomas may account for 22% and 36% of adenomas.^{14,15} Hence, there is a need for colorectal screening approaches that

offer improved sensitivity and specificity, especially for detection of flat and/or small lesions.

WLE is the current standard for colorectal cancer screening and one of the most commonly performed medical procedures in the United States.¹⁶ WLE has been shown to reduce mortality rates by as much as 50% in symptomatic patients.¹⁶ Although WLE can provide visualization of large-scale architectural and morphological features, it does not provide information coincident with early cancer development, such as changes in molecular composition or metabolic activity.¹⁷ In addition, the sensitivity and specificity of WLE is debated. Studies have estimated that the miss rates for large adenomas (≥ 10 mm) can range anywhere from 0% to 20%.^{18,19} A multicenter retrospective review estimated that the overall miss rate for colonic adenomas was 24% and for adenomas ≤ 5 mm, 27%.¹² However, there is also evidence for variance in sensitivity between endoscopists. A comprehensive review, performed by Rex, estimated that less-sensitive endoscopists may be missing the vast majority of colonic adenomas (miss rates as high as 90%).³ In addition to detection sensitivity, WLE has shown limited specificity in differentiating lesion histology. In a meta-analysis review, Ignjatovic et al.⁵ estimated that the accuracy

*Address all correspondence to: Silas J. Leavesley, E-mail: leavesley@southalabama.edu

for differentiating hyperplastic polyps and adenomas could range from 59% to 84% (Ref. 5 and references found therein: Refs. 7, 9, 20–23). Taken together, these data indicate a need for endoscopic technologies with improved sensitivity and specificity, as well as technologies or approaches that lead to reduced interoperator variation.

Several alternative endoscopic imaging modalities have been developed in an effort to increase detection sensitivity and specificity. Narrow-band imaging (NBI) utilizes optical filters with a narrow wavelength band to increase the contrast between an epithelial surface and the vascular pattern. This allows analysis of the surface epithelium and the underlying vascular network.^{20,24,25} Autofluorescence imaging (AFI) is an alternative approach for creating increased contrast in endoscopic images.^{26–31} AFI uses short-wavelength light or laser illumination to excite endogenous fluorophores within a tissue.^{32–36} In general, the autofluorescence intensity of cancerous and precancerous lesions is lower, due to mucosal thickening and reduced collagen fluorescence.²⁹ However, tissue autofluorescence has been attributed to many sources,³⁷ including metabolic molecules (NADH, FAD),^{38–40} proteins, and other molecules (flavins, collagen, elastin, hemoglobin),⁴¹ breakdown of certain biomolecules (hematoporphyrin, flavins),⁴² and induced molecular changes concurrent with inflammation.^{43–45} Hence, the molecular and histologic basis for AFI is still uncertain.

Several comparative studies have shown that NBI may provide increased sensitivity and specificity over conventional WLE^{5,6,8,11} and that AFI may provide increased sensitivity.^{11,46} Ignjatovic et al.⁵ compared the sensitivity, specificity, and accuracy of WLE to AFI, NBI, and NBI with magnification (NBImag) by using sequentially captured image sets of lesions and postprocedure scoring by expert and novice evaluators. Results revealed that both NBI and NBImag provided improved sensitivity, but reduced specificity, when compared to conventional WLE. Interestingly, AFI provided both reduced sensitivity and specificity.

Chromoendoscopy (CE) is a third alternative endoscopic imaging modality, which creates contrast by introducing topical labels (targeted dyes) into the visualized area through a working channel or injection port on the endoscope. Dyes or dye conjugates are selected to preferentially bind one or more types of tumor. Su et al.⁷ demonstrated a very high sensitivity of 95.7% using CE, with a specificity of 87.5%, and a diagnostic accuracy of 92.7%. Combining CE with pit pattern assessment may further raise diagnostic accuracy (85% to 96%).^{5,9,10,22,23,47} The drawbacks of CE—the additional labor and procedural times involved, requirement for specialized training, use of additional topical reagents (dyes), and the specificity of dyes across a wide range of tumor subtypes—have hindered wide-spread adoption of the technique.^{5,11,48–50}

Arguably, early and/or flat adenomas pose the most difficult detection challenge.^{17,37} None of the techniques discussed (WLE, NBI, AFI, and CE) provides a single fail-safe screening technology. Hence, there is a significant need for technologies that offer improved sensitivity and specificity, while maintaining normal procedure times and nominal procedure costs. One alternative detection approach may be through analysis of reflectance or fluorescence spectroscopic data. Both reflectance⁵¹ and fluorescence^{37,52} spectroscopy have been evaluated for their ability to detect colon cancers. In principle, the additional information provided by spectroscopic measurements should allow estimation of molecular composition as well as more

accurate detection sensitivity and specificity. For example, using a fluorescence spectroscopic approach, Cothren et al.⁵³ reported an incredibly high sensitivity of 100% and specificity of 97% for differentiating adenoma from normal mucosa and hyperplasia. A limitation of spectroscopic approaches is that only a single point-measurement is made, usually by inserting a fiber-optic probe through the working channel of the endoscope. Hence, this technique can be very tedious and time consuming, requiring the probe to be contacted with many locations of the mucosa to effectively locate the lesional border.

The goal of this preliminary study was to assess the potential feasibility of an alternative imaging technology^{54,55}—hyperspectral imaging with reflectance and fluorescence excitation scanning—for detecting differences between adenocarcinoma and surrounding normal tissue in resected colorectal cancer specimens. We have previously shown that hyperspectral imaging using fluorescence emission scanning can be used to accurately detect discrete molecular signals in cells and tissues.^{41,56–60} However, we have found that fluorescence excitation scanning provides 10- to 30-fold higher signal sensitivity than traditional (emission-based) spectral imaging approaches.⁵⁵ This technology allows fluorescence and absorbance image data to be acquired across a range of narrow-wavelength illumination bands, spanning the ultraviolet (UV) through visible spectrum and can easily be adapted for endoscopic use. We present initial data from four patients comparing fluorescence excitation spectral properties of cancerous to normal colon tissues, as well as a preliminary comparison of different structures within healthy colon and a brief discussion of effects of specimen preparation on measured excitation spectra. Initial results indicate that excitation-scanning hyperspectral imaging may be a viable technology for detecting spectral differences between normal and cancerous colon tissues.

2 Methods

2.1 Tissue Specimens

All studies were performed in conjunction with University of South Alabama Institutional Review Board protocol: IRB # 445452-3. Colorectal tissue samples were obtained by the University of South Alabama Departments of Surgery and Pathology from colorectal surgical resection specimens. The samples were collected as pairs of adenocarcinoma and normal mucosa and were ~0.5 to 1.0 mm in thickness. The tissues were flash frozen in liquid nitrogen. Confirmation of adenocarcinoma was determined by histologic evaluation of hematoxylin and eosin (H&E) permanent sections. Samples were maintained at -80°C until prior to hyperspectral imaging, typically within 1 to 2 days. For imaging, tissues were reconstituted in cold phosphate-buffered saline (PBS) and placed onto a 25-mm round coverslip.

A total of eight patients have been enrolled thus far in the study. However, data from the first three patients are not presented here, due to variations in specimen processing and imaging protocol. In addition, one patient was not considered, as surgical exam revealed extreme fibrosis, possibly due to perforation of the bowel, but no evidence of adenocarcinoma.

Fresh rat tissues were obtained postmortem from an ongoing, unrelated animal study. All procedures in the unrelated animal study were conducted in accordance with approved University of South Alabama Institutional Animal Care and Use Committee (IACUC) protocol #623125.

Table 1 Equipment settings for each type of hyperspectral imaging scan performed. Different dichroic beamsplitters were used to allow a range of fluorescence excitation scanning, with cut-off wavelengths at 458, 495, 555, and 594 nm cut-off wavelengths (part numbers: BLP01-458R-25, FF01-495/LP-25, BLP02-561R-25, and BLP01-594R-25, respectively, Semrock, Inc.). For transmission and absorbance scanning, no dichroic beamsplitter was used.

Type of scan	Dichroic beamsplitter cut-off wavelength (nm)	Starting wavelength (nm)	Ending wavelength (nm)	Step size (nm)
Fluorescence excitation	458	390	450	5
Fluorescence excitation	495	390	480	5
Fluorescence excitation	555	390	550	5
Fluorescence excitation	594	390	580	5
Transmission/absorbance	None	390	700	5

2.2 Hyperspectral Microscope

An inverted fluorescence microscope (TE2000-U, Nikon Instruments) with a 10× objective (10 × /.25 Ph1 ADL ∞/1.2 WD 6.2, Nikon Instruments) was used as the imaging platform. Illumination light was provided by a 300-W Xe arc lamp (TITAN 300ST-K, Sunoptics Technologies). An evaluation prototype thin-film tunable excitation filter system (Semrock, Inc.) containing six separate tunable filters (Versachrome, Semrock, Inc.) was used to filter the excitation light illuminating the sample. Our group has previously described this tunable filter system in detail.^{55,61,62} Output from the tunable filter

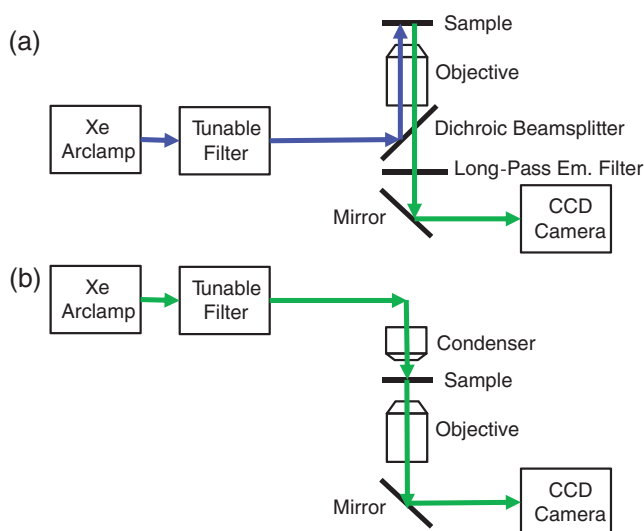


Fig. 1 Lightpaths for optical microscope setup: (a) fluorescence excitation-scanning mode and (b) transmission scanning mode. Note that when operating in fluorescence excitation-scanning mode, all fluorescence emission was detected using a long-pass emission filter, for each fluorescence excitation band used.

was coupled to the microscope through liquid light guide and supplied in either an epifluorescence configuration or a transmitted light configuration. An electron-multiplied charge-coupled device camera (Rolera-em-c², Q-Imaging) was used to acquire images of the illuminated tissues. For hyperspectral imaging, fluorescence excitation was scanned using four different wavelength ranges with corresponding long-pass dichroic beamsplitters at 458, 495, 555, and 594 nm cut-off wavelengths (Table 1). The optical path for the microscope in both fluorescence and reflectance configurations is shown in Fig. 1.

2.3 Image Acquisition

Fields of view within tissue specimens were identified for imaging using fluorescence with 480-nm excitation and 495-nm long-pass emission and transmission at 515 nm. Multiple fields of view were acquired to sample the range of structures in each specimen. An additional field of view was acquired that included the tissue edge and surrounding background region (with no tissue). The background spectrum was used during spectral correction (described below). All fluorescence hyperspectral images were acquired with the following detector settings: electron multiplying (EM) gain of 3800, 14-bit dynamic range, and binning of 2 × 2. Transmission images were acquired using an EM gain of 1. Image acquisition for each type of fluorescence and transmission spectral image stack was performed sequentially.

2.4 Image Processing and Analysis

Spectral images were postprocessed using MATLAB software (MathWorks). Absorbance data were calculated from transmission values, using the transmission spectrum from a background region as reference. ENVI software (Exelis Visual Information Solutions, Boulder, Colorado) was used to identify regions of interest (ROIs) and extract spectral data. Fluorescence images were corrected to flat spectral response using background subtraction and multiplication by a correction factor. Correction coefficients were determined using a NIST-traceable lamp (LS-1-CAL-INT, Ocean Optics, Inc.) and fiber-coupled spectrometer (QE65000, Ocean Optics, Inc.), as described previously.^{41,55,61}

Multiple ROIs were identified according to the structural features of each specimen. In addition, a region encompassing the entire field of view was selected. The average spectrum from each region was extracted. Extracted spectra were plotted using Excel (Office 2010, Microsoft Corporation).

2.5 Results and Discussion

Colonic adenocarcinoma and surrounding normal tissue were imaged using a hyperspectral imaging fluorescence excitation (HIFEX)-scanning microscope configuration. An example image of normal mucosa is shown in Fig. 2. For each pixel in the image, fluorescence excitation, transmission, and absorbance spectra were acquired [Figs. 2(a)–2(c)]. These images can be visualized as three-dimensional spectral image stacks, in which the first two dimensions represent spatial data and the third dimension represents spectral data. ROIs were selected based on structural/anatomical features in the image. For each ROI, the pixel-averaged spectrum was calculated for each hyperspectral imaging mode [Figs. 2(d)–2(h)]. In cases in which a desired structure of the specimen (e.g., mucosa)

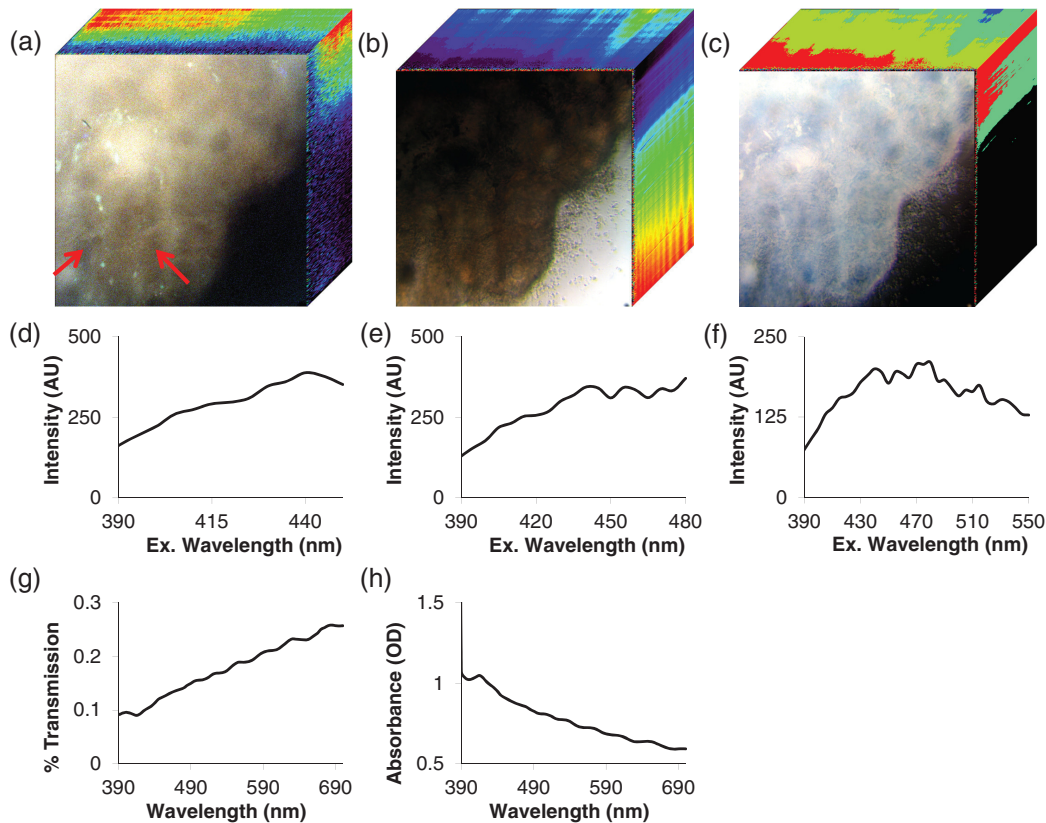


Fig. 2 Example image of normal colonic mucosa. For each pixel in the image, fluorescence excitation, transmission, and absorbance spectra were acquired. These images can be visualized as three-dimensional spectral image stacks, in which the first two dimensions represent spatial data and the third dimension represents spectral data. (a) HIFEX scan acquired from 390 to 480 nm. Three wavelength bands are shown for visualization (red = 465 nm, green = 430 nm, and blue = 390 nm). Spectral data are shown in the z-axis (going into the page). Arrows point to colonic crypts. (b) Transmission scan and (c) absorbance scan from 390 to 700 nm (red = 650 nm, green = 525 nm, and blue = 410 nm). (d–h) Pixel-averaged spectral data for a representative ROI: (d) fluorescence excitation scan from 390 to 450 nm, (e) fluorescence excitation scan from 390 to 480 nm (corresponding to the image in panel a), (f) fluorescence excitation scan from 390 to 550 nm, (g) transmission scan from 390 to 700 nm (corresponding to the image in panel b), and (h) absorbance scan from 390 to 700 nm (corresponding to the image in panel c).

spanned several fields of view, the spectra from multiple ROIs were averaged to obtain a representative spectral signature for the structure.

To assess tissue heterogeneity, vascular, adipose, and mucosal structures of noncancerous colon were imaged (Fig. 3). Different tissue structures had similar fluorescence spectral shapes with large differences in magnitude [Figs. 3(d)–3(e)], suggesting that the bulk fluorescence excitation spectrum of a healthy colon is homogeneous. However, normalizing fluorescence data to a peak value of unity [Figs. 3(g)–3(h)] revealed subtle differences, likely indicating that many autofluorescent molecules contribute to the overall spectrum. A possible explanation is that less stable autofluorescent molecules—such as NADH or FAD, whose fluorescence properties depend on the oxidative state of the molecule—may have been degraded or compromised during the flash freezing and sample preparation process.

Unfortunately, there are relatively few spectroscopic studies of tissue autofluorescence that report fluorescence excitation spectral data. Richards-Kortum and Sevick-Muraca³⁵ have reported flavomononucleotides, with a peak fluorescence excitation wavelength of 436 nm. However, Wagnieres et al.³⁷ (in a comprehensive review) have also reported that flavins

have a peak excitation wavelength of 455 nm and that porphyrins have a peak excitation wavelength of 400 nm. A definitive answer as to which molecules contribute to colon autofluorescence is not possible until a more detailed study of the components of fluorescence excitation spectra is performed. Further work is also warranted to develop specialized spectral analysis approaches that can identify weak signatures in the presence of much stronger signatures, such as matched filtering and energy minimization algorithms.^{63–65}

Interestingly, the absorbance data of colonic mucosa were much smaller, and of a different spectral shape, than that of vascular and adipose tissues [Figs. 3(f) and 3(i)]. This indicates that the composition of absorbing (but not fluorescing) molecules in the mucosa is different from that of vascular and adipose tissues. In addition, mucosa may be more transparent than either of the other tissue types and may allow a higher optical penetration depth, as indicated by the lower magnitude of absorbance. This observation indicates that absorbance or reflectance spectral image data may provide complimentary information to fluorescence spectral image data in differentiating among tissue types.

In this pilot study, four pairs of adenocarcinoma and surrounding normal mucosa were analyzed. While this is not a large enough sample size to calculate sensitivity and specificity

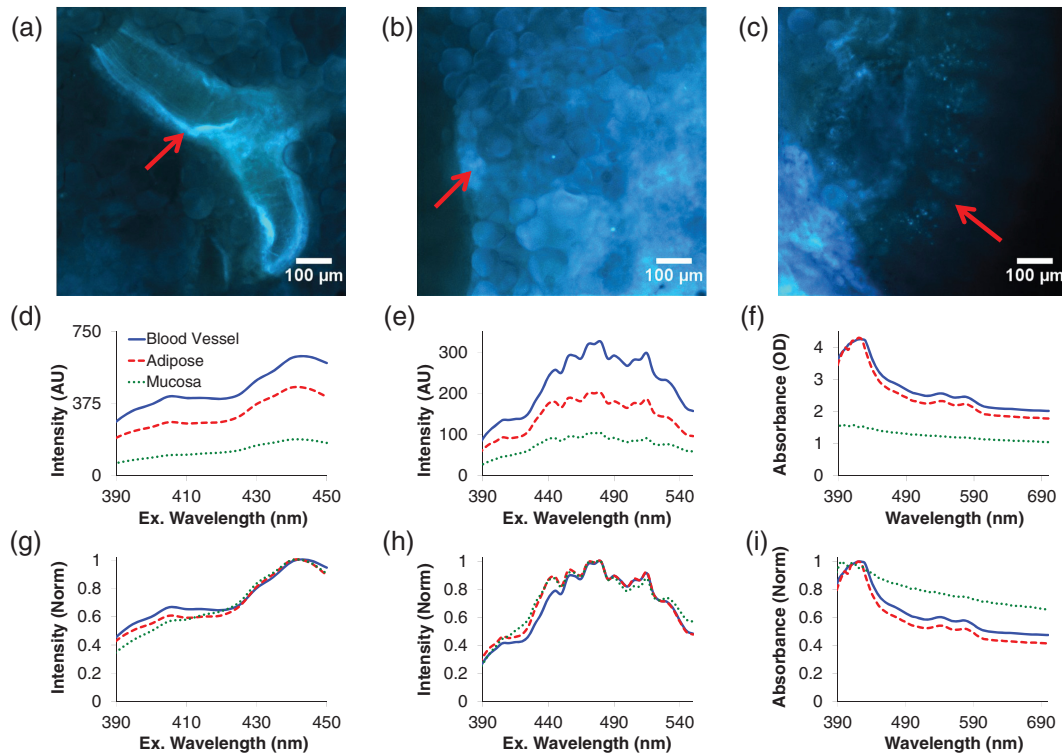


Fig. 3 Corrected images for three fields of view in normal tissue, showing (a) blood vessel, (b) adipose tissue, and (c) mucosa. Spectral data from the representative tissue types: (d) fluorescence excitation scan from 390 to 450 nm, (e) fluorescence excitation scan from 390 to 550 nm, (f) absorbance scan from 390 to 700 nm. Normalizing the fluorescence data to a peak value of unity (g and h) revealed that there may be subtle differences in the concentrations of two autofluorescent molecules, one with a peak excitation wavelength of 400 nm and another with a peak excitation wavelength of 440 nm. The absorbance spectrum of mucosa was smaller, and of a different shape, than that of vascular and adipose tissues (compare panels f and i), indicating the composition of absorbing molecules in the mucosa is different from that of vascular and adipose tissues. The heterogeneity in fluorescence and absorbance spectra is likely due to one or two autofluorescent molecules that are present at high concentrations, such as collagen or elastin, and additional autofluorescent molecules present at lower concentrations.

metrics, it does provide a proof-of-principle or early feasibility demonstration for visualizing differences in spectral signatures of cancerous and normal tissues. At short excitation wavelengths, the fluorescence total intensity of adenocarcinomas was lower than normal tissue [Fig. 4(a), data shown for two specimen pairs]. This is consistent with prior literature, which indicates that fluorescence emission decreases in colonic adenoma and carcinoma,^{29,53} as well as cancer progression in bronchial and oral mucosa.^{27,30} However, fluorescence resulting from excitation at higher wavelengths was increased, and in the S4 sample was higher than normal tissue [Figs. 4(b) and 4(c)]. Transmission and absorbance spectral data indicate that adenocarcinoma displays increased optical absorbance, as compared to surrounding normal tissue [Figs. 4(d) and 4(e)], with additional spectral differences that could be exploited to increase sensitivity and specificity for tumor detection. These preliminary data demonstrate that there may be differences in spectral signature (also called spectral fingerprint) between cancerous and normal tissue and indicate that the excitation-scanning approach could provide high specificity (and likely high sensitivity) for detecting adenocarcinomas. It is likely that hyperspectral imaging can detect subtle changes in spectral signatures coincident with cancer stage that may not be detectable

with NBI or AFI. In addition, due to the high sensitivity of fluorescence excitation-scanning hyperspectral imaging,⁵⁵ this technology could likely be translated to an endoscope or similar clinical imaging platform, enabling real-time hyperspectral imaging for endoscopy procedures. Finally, these data indicate that lesions are molecularly complex, likely heterogeneous, and should be investigated further to understand the relationship between cancer progression and spectral signature.

The wavelength range of 390 to 450 nm was selected to visualize key spectral differences for all specimen pairs (Fig. 5). For all tissue pairs, the fluorescence intensity of normal tissues was higher than cancerous tissues. This is consistent with prior literature that indicates that fluorescence emission decreases with adenocarcinoma,^{29,53} as well as bronchial and oral cancer.^{27,30} In addition, cancerous tissues presented several common spectral features, including a local peak excitation wavelength of 400 nm and a local minimum at 430 nm [Figs. 5(e) and 5(h)]. This indicates that adenocarcinomas have common aspects of molecular composition.

It is currently not clear which molecules contributed to changes in the fluorescence excitation spectrum of adenocarcinomas. Zângaro et al.⁶⁶ reported a similar peak excitation wavelength of 440 to 450 nm but did not attribute this to a specific

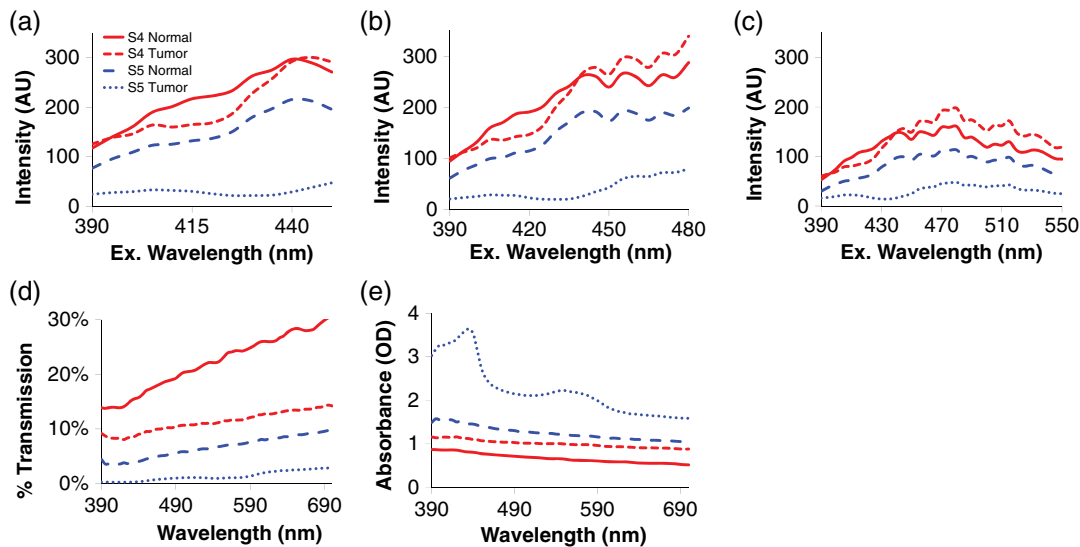


Fig. 4 Spectral differences between normal and cancerous tissue for two specimen pairs: S4 and S5. Preliminary data demonstrate the differences in spectral signature (fingerprint) between cancerous and normal tissue. Transmission and absorbance spectral data indicate that adenocarcinoma displays increased optical absorbance, as compared to surrounding normal tissue, with additional spectral differences that could be exploited to increase sensitivity and specificity for tumor detection. Spectral scan types are as follows: (a) fluorescence excitation scan from 390 to 450 nm, (b) fluorescence excitation scan from 390 to 450 nm, (c) fluorescence excitation scan from 390 to 450 nm, (d) transmission scan from 390 to 700 nm, and (e) absorbance scan from 390 to 700 nm.

molecule. Wagnier et al.³⁷ summarized fluorescence excitation data, indicating that flavins have peak excitation wavelengths at 380 and 460 nm. In addition, lipopigments were reported to have a secondary excitation peak at 440 nm. By contrast, NADH was reported to have lower peak excitation wavelengths, at 260 and 350 nm. However, the fluorescence excitation spectrum of tissues has been reported only in a small number of studies, and even fewer studies have measured the fluorescence excitation spectrum from the UV through the visible range. Hence, future work is needed to study autofluorescence molecules under a broad range of fluorescence excitation wavelengths.

In the long term, a spectral library of fluorescence excitation spectra could be used to assist physicians in the diagnostic process in several ways: (1) by providing an estimate of tissue composition for specified areas of interest, (2) by providing molecular maps of a tissue using linear unmixing^{67,68} or other spectral analysis technique,^{69–71} (3) by allowing calculation of derived maps (such as redox ratio^{72,73} or blood oxygen saturation^{74–76}), which may correlate with cancer development. If unmixing or spectral analysis is performed, it may be advantageous to employ more sophisticated nonlinear unmixing approaches, especially if reflectance and fluorescence image data can be combined to better estimate tissue parameters, such as scatter.⁷⁷ Regardless of the algorithm employed, the ability to visualize spectrally analyzed “molecular maps” during endoscopic navigation could improve the ability to detect small lesions and delineate the margins of larger lesions.

An advantage of fluorescence excitation scanning is that it can offer a large increase in signal strength.⁵⁵ As shown in Fig. 1(a), there is no need to spectrally resolve the fluorescence emission, as long as there is clean separation of the emission from excitation light using an appropriate long-pass

fluorescence emission filter. In this configuration, all of the fluorescence emission is detected in a single long-pass emission channel for each excitation wavelength band, greatly increasing the signal strength. The increased signal strength can, in turn, allow proportional increases in imaging speed. In addition, the microscope configuration used for this study lends itself to an endoscope design in which fluorescence and reflectance may be measured simultaneously (Fig. 6). A future endoscope system using this design would provide identical fluorescence information as the microscope lightpath used in this study, but would be limited to measuring spectral reflectance instead of transmission. However, due to the increased signal strength provided by the fluorescence excitation-scanning approach and due to the ability to simultaneously measure fluorescence and reflectance, it is likely that this technology could be implemented in real time for screening during an endoscopy procedure.

It should be noted that images of transmission or reflectance represent combined characteristics of the tissue, at the point of measurement. Even in current endoscopes, reflected light images are likely affected by several terms, including wavelength-dependent variations in refractive index of the tissue. Hence, for the case of transmission- or reflectance-based spectral imaging, the measured spectrum represents the composite effects of absorption, scatter, anisotropy, and wavelength-dependent refractive index changes. Many of these parameters have previously been shown to be heterogeneous across tissue types.⁷⁷ Hence, the basis for detecting colorectal lesions using reflectance-based spectral imaging would incorporate these variations, even if only from a lumped-parameter perspective.

Tissue preparation and/or fixation may affect the spectral properties and hence, the perceived feasibility of excitation-scanning hyperspectral imaging for colorectal screening. As

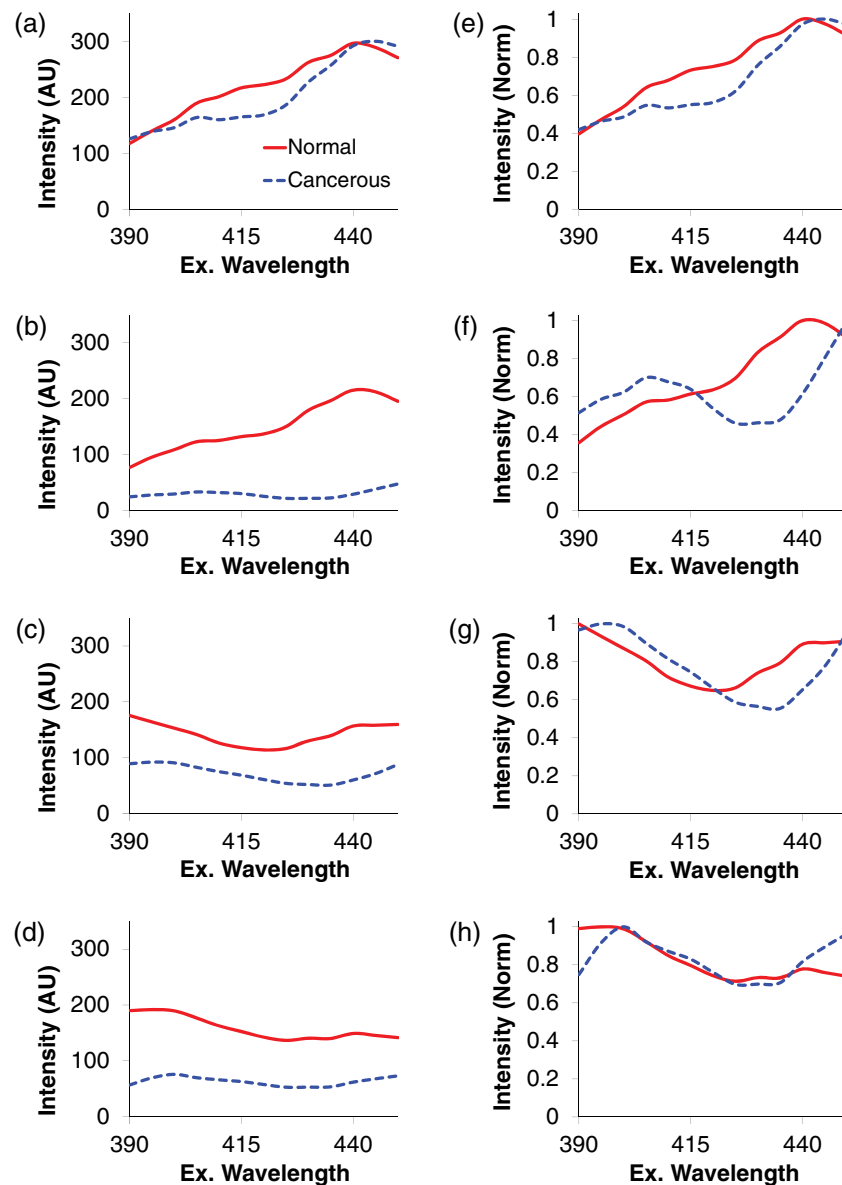


Fig. 5 Fluorescence excitation scans from 390 to 450 nm of normal mucosa (solid red line) and adenocarcinoma (dashed blue line) from four patients. The total fluorescence excitation intensity (magnitude) of adenocarcinomas is lower than normal mucosa. In addition, adenocarcinomas present several characteristic spectral features, which normalized to a peak value of unity, including a local peak at 400 nm and a local minimum at 430 nm. These differences in spectral signature (fingerprint) offer a potential approach for discriminating cancerous and noncancerous tissues with high accuracy. (a–d) Raw spectra, corrected to NIST-traceable response. (e–h) Spectra normalized to a peak value of unity.

an example, we compared spectra from the tissue specimens used in this study to similar colon tissues isolated from rats, which were discarded upon completion of an unrelated study. The tissue specimens used in this study were resected during surgical procedure, screened by pathology, flash-frozen in liquid nitrogen for transport, and then thawed in cold PBS prior to imaging. By contrast, the fresh rat colon tissues were obtained immediately after euthanizing the animal and stored in cold PBS for no more than 3 h prior to imaging. While the tissues were obtained from different sources, results indicate that there may be additional spectral components present in nonfrozen tissues that are lost during the tissue freezing and thawing process (Fig. 7). Further studies are warranted to quantify the effects of

tissue freezing, as well as tissue fixation, on autofluorescence spectra.

3 Conclusion

In this pilot study, we present data indicating that fluorescence excitation-scanning hyperspectral imaging offers an alternative approach that may be feasible for identifying adenocarcinoma of the colon. From the initial cohort of four patients, adenocarcinomas presented consistency among spectral features within the wavelength range of 390 to 450 nm. Unfortunately, few spectroscopic studies of tissue autofluorescence report fluorescence excitation spectral data,^{35,37} and the exact molecular composition of each tissue type is yet to be determined. These

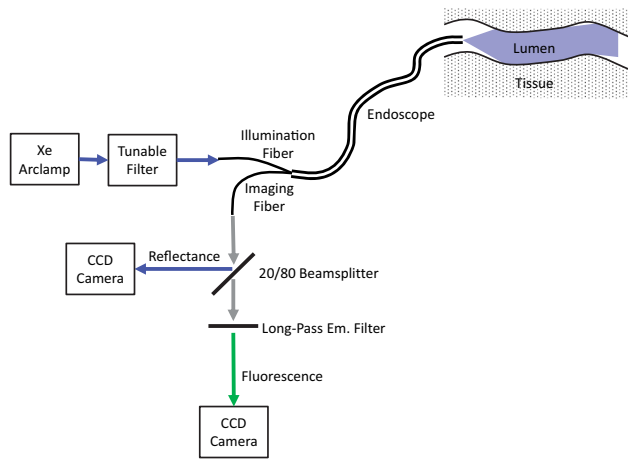


Fig. 6 Potential optical design for a future spectral imaging endoscope based on the fluorescence excitation-scanning technology. Both fluorescence excitation spectral images and reflectance spectral images may be acquired simultaneously. Note that a future endoscope design would likely be limited to measuring spectral reflectance, instead of transmittance, due to the inability to place the illumination and detector on opposite sides of the lumen wall.

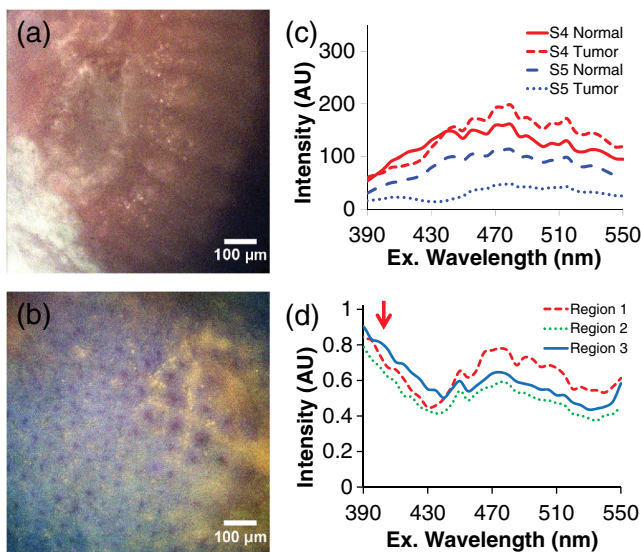


Fig. 7 Spectral artifacts may be introduced during flash freezing and thawing, resulting in reduced molecular discrimination. (a) Example of a false-colored spectral image of flash-frozen human colorectal tissue specimen from this pilot study (transverse view); (b) false-colored spectral image of fresh (nonfrozen) rat colon from an ongoing animal study (en-face view); (c) average spectra from cancerous and normal tissue from two patients; (d) average spectra from three ROIs selected from the image in panel b. The red arrow indicates additional spectral components that are present in the fresh tissue and were likely lost during the flash freezing and thawing process.

preliminary data indicate that the excitation-scanning approach could be effective for detecting differences in spectral signature concurrent with cancer development (Fig. 5). However, further studies are needed to verify these results using a larger patient base, to estimate the sensitivity and specificity of this approach, and to determine the molecular contributors to mucosal autofluorescence.

Acknowledgments

The authors would like to acknowledge support from NIH under Grant Nos. UL1 TR001417 and P01 HL066299, the University of Alabama at Birmingham Center for Clinical and Translational Science (CCTS), and the Abraham Mitchell Cancer Research Fund. We would also like to acknowledge use of the evaluation thin-film tunable filter system, provided by Semrock, Inc., a unit of IDEX. Drs. Rich and Leavesley disclose financial interest in a start-up company, SpectraCyte, for commercializing spectral imaging technologies. Some of the results in this paper have been also described in a corresponding SPIE Photonics West conference proceedings, paper #970315.⁷⁸

References

1. A. Jemal et al., "Cancer statistics, 2008," *CA Cancer J. Clin.* **58**(2), 71–96 (2008).
2. L. A. G. Ries et al., *SEER Cancer Statistics Review, 1975–2005*, pp. 1975–2005, National Cancer Institute, Bethesda MD (2008).
3. D. K. Rex, "Maximizing detection of adenomas and cancers during colonoscopy," *Am. J. Gastroenterol.* **101**(12), 2866–2877 (2006).
4. P. A. Newcomb et al., "Screening sigmoidoscopy and colorectal cancer mortality," *J. Natl. Cancer Inst.* **84**(20), 1572–1575 (1992).
5. A. Ignjatovic et al., "What is the most reliable imaging modality for small colonic polyp characterization? Study of white-light, autofluorescence, and narrow-band imaging," *Endoscopy* **43**(2), 94–99 (2011).
6. T. Matsumoto et al., "Chromoendoscopy, narrow-band imaging colonoscopy, and autofluorescence colonoscopy for detection of diminutive colorectal neoplasia in familial adenomatous polyposis," *Dis. Colon Rectum* **52**(6), 1160–1165 (2009).
7. M.-Y. Su et al., "Comparative study of conventional colonoscopy, chromoendoscopy, and narrow-band imaging systems in differential diagnosis of neoplastic and nonneoplastic colonic polyps," *Am. J. Gastroenterol.* **101**(12), 2711–2716 (2006).
8. H.-M. Chiu et al., "A prospective comparative study of narrow-band imaging, chromoendoscopy, and conventional colonoscopy in the diagnosis of colorectal neoplasia," *Gut* **56**(3), 373–379 (2007).
9. G. D. De Palma et al., "Conventional colonoscopy and magnified chromoendoscopy for the endoscopic histological prediction of diminutive colorectal polyps: a single operator study," *World J. Gastroenterol.* **12**(15), 2402–2405 (2006).
10. K. Togashi et al., "A comparison of conventional endoscopy, chromoendoscopy, and the optimal-band imaging system for the differentiation of neoplastic and non-neoplastic colonic polyps," *Gastrointest. Endosc.* **69**(3), 734–741 (2009).
11. F. J. van den Broek et al., "Endoscopic tri-modal imaging for surveillance in ulcerative colitis: randomised comparison of high-resolution endoscopy and autofluorescence imaging for neoplasia detection; and evaluation of narrow-band imaging for classification of lesions," *Gut* **57**(8), 1083–1089 (2008).
12. D. K. Rex et al., "Colonoscopic miss rates of adenomas determined by back-to-back colonoscopies," *Gastroenterology* **112**(1), 24–28 (1997).
13. K. Imaizumi et al., "Dual-wavelength excitation of mucosal autofluorescence for precise detection of diminutive colonic adenomas," *Gastrointest. Endosc.* **75**(1), 110–117 (2012).
14. Y. Saitoh et al., "Prevalence and distinctive biologic features of flat colorectal adenomas in a North American population," *Gastroenterology* **120**(7), 1657–1665 (2001).
15. B. Rembacken et al., "Flat and depressed colonic neoplasms: a prospective study of 1000 colonoscopies in the UK," *Lancet* **355**(9211), 1211–1214 (2000).
16. L. C. Seeff et al., "How many endoscopies are performed for colorectal cancer screening? Results from CDC's survey of endoscopic capacity," *Gastroenterology* **127**(6), 1670–1677 (2004).
17. R. T. Kester et al., "Real-time snapshot hyperspectral imaging endoscope," *J. Biomed. Opt.* **16**(5), 056005 (2011).
18. L. Hixson et al., "Prospective blinded trial of the colonoscopic miss rate of large colorectal polyps," *Gastrointest. Endosc.* **37**(2), 125–127 (1991).

19. P. Schoenfeld et al., "Accuracy of polyp detection by gastroenterologists and nurse endoscopists during flexible sigmoidoscopy: a randomized trial," *Gastroenterology* **117**(2), 312–318 (1999).
20. H. Machida et al., "Narrow-band imaging in the diagnosis of colorectal mucosal lesions: a pilot study," *Endoscopy* **36**(12), 1094–1098 (2004).
21. D. Apel et al., "Accuracy of high-resolution chromoendoscopy in prediction of histologic findings in diminutive lesions of the rectosigmoid," *Gastrointest. Endosc.* **63**(6), 824–828 (2006).
22. K. Fu et al., "Chromoendoscopy using indigo carmine dye spraying with magnifying observation is the most reliable method for differential diagnosis between non-neoplastic and neoplastic colorectal lesions: a prospective study," *Endoscopy* **36**(12), 1089–1093 (2004).
23. J. Tischendorf et al., "Value of magnifying chromoendoscopy and narrow band imaging (NBI) in classifying colorectal polyps: a prospective controlled study," *Endoscopy* **39**(12), 1092–1096 (2007).
24. K. Gono et al., "Endoscopic observation of tissue by narrowband illumination," *Opt. Rev.* **10**(4), 211–215 (2003).
25. K. Gono et al., "Appearance of enhanced tissue features in narrow-band endoscopic imaging," *J. Biomed. Opt.* **9**(3), 568–577 (2004).
26. R. Alfano et al., "Laser induced fluorescence spectroscopy from native cancerous and normal tissue," *IEEE J. Quantum Electron.* **20**(12), 1507–1511 (1984).
27. J. Hung et al., "Autofluorescence of normal and malignant bronchial tissue," *Lasers Surg. Med.* **11**(2), 99–105 (1991).
28. R. Adachi, T. Utsui, and K. Furusawa, "Development of the autofluorescence endoscope imaging system," *Diagn. Ther. Endosc.* **5**(2), 65–70 (1999).
29. K. Izuishi et al., "The histological basis of detection of adenoma and cancer in the colon by autofluorescence endoscopic imaging," *Endoscopy* **31**(7), 511–516 (1999).
30. C. Betz et al., "Autofluorescence imaging and spectroscopy of normal and malignant mucosa in patients with head and neck cancer," *Lasers Surg. Med.* **25**(4), 323–334 (1999).
31. G. W. Falk, "Autofluorescence endoscopy," *Gastrointest. Endosc. Clin. N. Am.* **19**(2), 209–220 (2009).
32. R. S. DaCosta, H. Andersson, and B. C. Wilson, "Molecular fluorescence excitation-emission matrices relevant to tissue spectroscopy," *Photochem. Photobiol.* **78**(4), 384–392 (2003).
33. R. S. DaCosta, B. C. Wilson, and N. E. Marcon, "Optical techniques for the endoscopic detection of dysplastic colonic lesions," *Curr. Opin. Gastroenterol.* **21**(1), 70–79 (2005).
34. F. J. van den Broek et al., "Combining autofluorescence imaging and narrow-band imaging for the differentiation of adenomas from non-neoplastic colonic polyps among experienced and non-experienced endoscopists," *Am. J. Gastroenterol.* **104**(6), 1498–1507 (2009).
35. R. Richards-Kortum and E. Sevick-Muraca, "Quantitative optical spectroscopy for tissue diagnosis," *Annu. Rev. Phys. Chem.* **47**, 555–606 (1996).
36. D. Pantalone et al., "Multispectral imaging autofluorescence microscopy in colonic and gastric cancer metastatic lymph nodes," *Clin. Gastroenterol. Hepatol.* **5**(2), 230–236 (2007).
37. G. A. Wagnieres, W. M. Star, and B. C. Wilson, "In vivo fluorescence spectroscopy and imaging for oncological applications," *Photochem. Photobiol.* **68**(5), 603–632 (1998).
38. B. Chance et al., "Oxidation-reduction ratio studies of mitochondria in freeze-trapped samples. NADH and flavoprotein fluorescence signals," *J. Biol. Chem.* **254**(11), 4764–4771 (1979).
39. R. Drezek et al., "Understanding the contributions of NADH and collagen to cervical tissue fluorescence spectra: modeling, measurements, and implications," *J. Biomed. Opt.* **6**(4), 385–396 (2001).
40. I. Pavlova et al., "Microanatomical and biochemical origins of normal and precancerous cervical autofluorescence using laser-scanning fluorescence confocal microscopy," *Photochem. Photobiol.* **77**(5), 550–555 (2003).
41. S. J. Leavesley et al., "Hyperspectral imaging microscopy for identification and quantitative analysis of fluorescently-labeled cells in highly autofluorescent tissue," *J. Biophotonics* **5**(1), 67–84 (2012).
42. D. Chorvat, Jr. et al., "Spectral unmixing of flavin autofluorescence components in cardiac myocytes," *Biophys. J.* **89**(6), L55–L57 (2005).
43. J. Haringsma et al., "Autofluorescence endoscopy: feasibility of detection of GI neoplasms unapparent to white light endoscopy with an evolving technology," *Gastrointest. Endosc.* **53**(6), 642–650 (2001).
44. I. Pavlova et al., "Understanding the biological basis of autofluorescence imaging for oral cancer detection: high-resolution fluorescence microscopy in viable tissue," *Clin. Cancer Res.* **14**(8), 2396–2404 (2008).
45. A. Samy et al., "Role of autofluorescence in inflammatory/infective diseases of the retina and choroid," *J. Ophthalmol.* **2014**, 1–9(2014).
46. D. Ramsioek et al., "A back-to-back comparison of white light video endoscopy with autofluorescence endoscopy for adenoma detection in high-risk subjects," *Gut* **59**(6), 785–793 (2010).
47. D. Hurlstone, "High-resolution magnification chromoendoscopy: common problems encountered in 'pit pattern' interpretation and correct classification of flat colorectal lesions," *Am. J. Gastroenterol.* **97**(4), 1069–1070 (2002).
48. F. J. van den Broek, P. Fockens, and E. Dekker, "Review article: new developments in colonic imaging," *Aliment. Pharmacol. Ther.* **26**(s2), 91–99 (2007).
49. S.-E. Kudo et al., "Diagnosis of colorectal tumorous lesions by magnifying endoscopy," *Gastrointest. Endosc.* **44**(1), 8–14 (1996).
50. K. Togashi et al., "Efficacy of magnifying endoscopy in the differential diagnosis of neoplastic and non-neoplastic polyps of the large bowel," *Dis. Colon Rectum* **42**(12), 1602–1608 (1999).
51. G. Zonios et al., "Diffuse reflectance spectroscopy of human adenomatous colon polyps *in vivo*," *Appl. Opt.* **38**(31), 6628–6637 (1999).
52. S. Andersson-Engels et al., "Fluorescence imaging and point measurements of tissue: applications to the demarcation of malignant tumors and atherosclerotic lesions from normal tissue," *Photochem. Photobiol.* **53**(6), 807–814 (1991).
53. R. M. Cothren et al., "Gastrointestinal tissue diagnosis by laser-induced fluorescence spectroscopy at endoscopy," *Gastrointest. Endosc.* **36**(2), 105–111 (1990).
54. S. J. Leavesley et al., "An excitation wavelength-scanning spectral imaging system for preclinical imaging," *Rev. Sci. Instrum.* **79**(2), 023707–023710 (2008).
55. P. F. Favreau et al., "Excitation-scanning hyperspectral imaging microscope," *J. Biomed. Opt.* **19**(4), 046010 (2014).
56. S. Leavesley et al., "Multispectral imaging analysis: spectral deconvolution and applications in biology," *Proc. SPIE* **5699**, 121 (2005).
57. N. S. Annamdevula et al., "An approach for characterizing and comparing hyperspectral microscopy systems," *Sensors* **13**(7), 9267–9293 (2013).
58. S. J. Leavesley et al., "Assessing FRET using spectral techniques," *Cytometry A* **83**(10), 898–912 (2013).
59. T. C. Rich et al., "Hyperspectral imaging of FRET-based cGMP probes," in *Guanylate Cyclase and Cyclic GMP: Methods and Protocols*, 1st ed., T. Krieg and R. Lukowski, Eds., Vol. **1020**, pp. 73–88, Springer Science + Business Media, LLC, New York (2013).
60. S. J. Leavesley et al., "Automated Image Analysis of FRET Signals for Subcellular cAMP Quantification," in *cAMP Signaling: Methods and Protocols*, M. Zaccolo, Ed., Vol. **1294**, pp. 59–70, Springer, New York, New York (2015).
61. P. F. Favreau et al., "Thin-film tunable filters for hyperspectral fluorescence microscopy," *J. Biomed. Opt.* **19**(1), 011017 (2014).
62. P. F. Favreau et al., "Tunable thin-film optical filters for hyperspectral microscopy," *Proc. SPIE* **8589**, 85890R (2013).
63. A. P. Williams and E. R. Hunt Jr., "Estimation of leafy spurge cover from hyperspectral imagery using mixture tuned matched filtering," *Remote Sens. Environ.* **82**(2–3), 446–456 (2002).
64. W. H. Farrand and J. C. Harsanyi, "Mapping the distribution of mine tailings in the Coeur d'Alene River Valley, Idaho, through the use of a constrained energy minimization technique," *Remote Sens. Environ.* **59**(1), 64–76 (1997).
65. D. Frolov and R. B. Smith, "Locally adaptive constrained energy minimization for aviris image," *Eighth JPL Airborne Earth Science (AVIRS)*, (1999) <http://www.microimages.com/papers> (17 October 2016).
66. R. A. Zangaro et al., "Rapid multiexcitation fluorescence spectroscopy system for *in vivo* tissue diagnosis," *Appl. Opt.* **35**(25), 5211–5219 (1996).
67. N. Keshava and J. F. Mustard, "Spectral unmixing," *IEEE Signal Process Mag.* **19**(1), 44–57 (2002).
68. N. Keshava, "A survey of spectral unmixing algorithms," *Linc. Lab. J.* **14**(1), 55–78 (2003).

69. C. I. Chang, *Hyperspectral imaging: Techniques for Spectral Detection and Classification*, Kluwer Academy, Plenum Publishers, New York (2003).
70. J. A. Richards, *Remote Sensing Digital Image Analysis: An Introduction*, 5th ed., Springer-Verlag (1999).
71. R. A. Schowengerdt, *Remote Sensing: Models and Methods for Image Processing*, Academic Press, San Diego, California (2006).
72. I. Quesada, M. G. Todorova, and B. Soria, "Different metabolic responses in α -, β -, and δ -cells of the islet of langerhans monitored by redox confocal microscopy," *Biophys. J.* **90**(7), 2641–2650 (2006).
73. R. Sepehr et al., "Optical imaging of tissue mitochondrial redox state in intact rat lungs in two models of pulmonary oxidative stress," *J. Biomed. Opt.* **17**(4), 046010 (2012).
74. E. Merrick and T. Hayes, "Continuous, non-invasive measurements of arterial blood oxygen levels," *Hewlett-Packard J.* **28**(2), 2–9 (1976).
75. I. Yoshiya, Y. Shimada, and K. Tanaka, "Spectrophotometric monitoring of arterial oxygen saturation in the fingertip," *Med. Biol. Eng. Comput.* **18**(1), 27–32 (1980).
76. M. Nitzan and S. Engelberg, "Three-wavelength technique for the measurement of oxygen saturation in arterial blood and in venous blood," *J. Biomed. Opt.* **14**(2), 024046 (2009).
77. V. V. Tuchin, *Tissue Optics: Light Scattering Methods and Instruments for Medical Diagnosis*, 2nd ed., SPIE Press, Bellingham (2007).
78. S. J. Leavesley et al., "Hyperspectral imaging fluorescence excitation scanning for detecting colorectal cancer: pilot study," *Proc. SPIE* **9703**, 970315 (2016).

Silas J. Leavesley received his BSc degree in chemical engineering in 2003 from Florida State University and his PhD in biomedical engineering in 2008 from Purdue University. Currently, he is an associate professor in the Departments of Chemical and Biomolecular Engineering, Pharmacology, and the Center for Lung Biology at the University of South Alabama. His research interests lie in the development of spectral imaging technologies for medical sciences research and clinical applications.

Mikayla Walters is a senior chemical engineering student at the University of South Alabama. She worked in the Leavesley-Rich Lab the summer after her freshman year, and since she has been

studying heterogeneous catalysis for fuel cell applications with Dr. Christy Wheeler West. She plans to complete an engineering internship in Chile this summer before starting her master's in chemical engineering at USA in fall 2017.

Peter F. Favreau received his BS degree in physics in 2010, and his PhD in basic medical sciences–biomedical engineering track in 2015 from the University of South Alabama. Currently, he is a postdoctoral fellow at the Morgridge Institute for Research in Madison, Wisconsin. His research focuses on the development of rapid imaging platforms for drug discovery in cancer therapy and beyond. Specifically, using fluorescence lifetime approaches to quickly determine drug efficacy "at-a-glance" for personalized cancer therapies.

Thomas C. Rich received his BAE and MS degrees in aerospace engineering from Georgia Institute of Technology in 1988 and 1990, respectively, and his PhD in biomedical engineering from Vanderbilt University in 1996. Currently, he is a professor in the Department of Pharmacology and Center of Lung Biology at the University of South Alabama. His research interests include the implementation of spectral imaging approaches for both basic and translational research.

Paul F. Rider is an associate professor in the Department of Surgery, and Chief of the Division of Colorectal Surgery. He also serves as associate program director of the Surgery Residency Program. He is board certified in both general and colorectal surgery. He is a fellow in the American College of Surgeons and the American Society of Colorectal Surgery. He is actively engaged in medical research and community service.

Carole W. Boudreaux graduated from Louisiana State University School of Medicine in Shreveport, Louisiana in 1990. She completed a combined anatomic and clinical pathology residency at the University of South Alabama in Mobile, Alabama, in 1995. She is certified in anatomic and clinical pathology by the American Board of Pathology with added certification in cytopathology. Currently, she is an associate professor in the Department of Pathology at the University of South Alabama.

Biographies for the authors are not available.